Short-wavelength optoacoustic spectroscopy based on water muting

Jaya Prakash[a,b,1], Mir Mehdi Seyedebrahimi[a,1], Ara Ghazaryan[a,1], Jaber Malekzadeh-Najafabadi[a], Vipul Gujrati[a], and Vasilis Ntziachristos[a,c,2]

[a]Institute of Biological and Medical Imaging, Helmholtz Zentrum München, D-85764 Neuherberg, Germany; [b]Department of Instrumentation and Applied Physics, Indian Institute of Science, Bangalore 560 012, India; and [c]Chair of Biological Imaging and TranslaTUM, Technical University of Munich, D-81675 Munich, Germany

Edited by Alexis T. Bell, University of California, Berkeley, CA, and approved January 14, 2020 (received for review June 25, 2019)

Infrared (IR) optoacoustic spectroscopy can separate a multitude of molecules based on their absorption spectra. However, the technique is limited when measuring target molecules in aqueous solution by strong water absorption at IR wavelengths, which reduces detection sensitivity. Based on the dependence of optoacoustic signal on the temperature of the probed medium, we introduce cooled IR optoacoustic spectroscopy (CIROAS) to mute water contributions in optoacoustic spectroscopy. We showcase that spectral measurements of proteins, lipids, and glucose in the short-wavelength IR region, performed at 4 °C, lead to marked sensitivity improvements over conventional optoacoustic or IR spectroscopy. We elaborate on the dependence of optoacoustic signals on water temperature and demonstrate polarity changes in the recorded signal at temperatures below 4 °C. We further elucidate the dependence of the optoacoustic signal and the muting temperature on sample concentration and demonstrate that changes in these dependences enable quantification of the solute concentration. We discuss how CIROAS may enhance abilities for molecular sensing in the IR.

sensing | photoacoustics | near infrared | temperature | spectroscopy

Measurement of proteins, lipids, collagen, and sugars is essential in biomedical research and diagnostics or therapeutics (1–7) and can lead to differentiating healthy from diseased tissues (8–11). Several tissue biomolecules exhibit absorption of light in the ultraviolet (UV), visible, and infrared (IR) ranges and therefore can be detected by optical spectroscopy (OS) (12, 13). Nevertheless, despite wide utilization in determining concentrations of chromophores, OS of many intrinsic tissue biomolecules comes with various disadvantages that depend on the wavelength range employed. UV wavelengths cause photodamage in biological samples, while visible and near infrared (NIR) wavelengths provide relatively poor sensitivity for lipids, sugars, and proteins (14, 15). Longer wavelengths, such as those in the short wavelength infrared (SWIR, 900 to 1,800 nm), offer detection of endogenous molecules such as proteins, lipids, and sugars with higher contrast, but the sensitivity of the technique is limited by the absorption of water (12–15).

To avoid the problem of water absorption, it is common to tag target biomolecules with fluorescent labels in order to increase detection sensitivity (16). Raman spectroscopy is also considered as it detects symmetric vibrations of nonpolar molecules and therefore is insensitive to water absorption. Although Raman spectroscopy can be performed at the UV, visible, and IR wavelengths, the UV and visible regimes are heavily influenced by background autofluorescence in tissues (5, 17). In fact, even weak fluorescence is much stronger than the generated Raman signal (17), which is why ultrasensitive trace detection is typically performed based on fluorescence (requires 10^{-16} cm^2 per molecule) rather than Raman spectroscopy (requires 10^{-30} to 10^{-25} cm^2 per molecule) (17, 18). Therefore, longer wavelengths are preferred for Raman sensing. Nevertheless, Raman scattering by biological samples generally leads to low signal-to-noise ratios (SNRs) for detailed studies, reflecting the fact that usually only 1 in 10^{10} photons undergoes a Stokes or anti-Stokes shift (10, 17, 18). The Raman signal can be strengthened by increasing light intensity, but this leads to photodamage. Alternatively, significant detection improvement can be achieved by bringing molecules in close proximity to metallic nanostructures in so-called surface-enhanced Raman spectroscopy (18).

Optoacoustic spectroscopy has also been considered for characterizing a range of biologically relevant chromophores in aqueous environments, including hemoglobin, melanin, or contrast agents such as gold nanoparticles and organic dyes (19–23) and in analytical chemistry and nanomedicine applications (24, 25). The method detects the emission of sound waves from target molecules following absorption of incident light of transient intensity. Nevertheless, similarly to optical methods, optoacoustic sensing is limited by water absorption at longer wavelengths. Water contributes minimally to optoacoustic measurements in the visible range (450 to 650 nm) and NIR range (650 to 900 nm) (14), but it contributes strongly to measurements at wavelengths longer than 900 nm, limiting the sensitivity of the technique for detecting proteins, lipids, collagen, and sugars (14, 26, 27). Measurements

Significance

Infrared (IR) optoacoustic spectroscopy is limited when measuring target molecules in aqueous solution by strong water absorption at IR wavelengths, which reduces detection sensitivity. In this work, we explored the dependence of optoacoustic signal on the temperature of the probed medium and introduced cooled IR optoacoustic spectroscopy (CIROAS) to mute water contributions while performing optoacoustic spectroscopy. We showcase that spectral measurements of proteins, lipids, and glucose in the short-wavelength IR region, performed at 4 °C, lead to marked sensitivity improvements over conventional optoacoustic or IR spectroscopy. CIROAS can enable a spectroscopic approach with high dissemination potential, offering a straightforward way to improve the sensitivity of detection of various molecules in biological samples.

Author contributions: J.P. and V.N. designed research; J.P., M.M.S., A.G., J.M.-N., and V.G. performed research; J.P., M.M.S., A.G., and V.N. analyzed data; and J.P. and V.N. wrote the paper.

Competing interest statement: V.N. is an equity owner in and consultant for iThera Medical GmbH, Munich, Germany; a member of the scientific advisory board of SurgVision BV/Bracco Sp. A, Groningen, The Netherlands; and the owner of Spear UG, Munich, Germany.

This article is a PNAS Direct Submission.

Data deposition: The data used in this paper have been deposited at Open Science Framework (https://osf.io/kt853/), and the corresponding codes to analyze the data have been deposited on GitHub (https://github.com/pnjayaprakash88/CIROAS_Spectroscopy).

[1]J.P., M.M.S., and A.G. contributed equally to this work.

[2]To whom correspondence may be addressed. Email: vntziachristos@gmail.com.

This article contains supporting information online at https://www.pnas.org/lookup/suppl/doi:10.1073/pnas.1910597117/-/DCSupplemental.

First published February 6, 2020.

of the optical absorption spectrum of glucose and lipids have been previously performed (14, 28), albeit with low sensitivity due to the strong absorption by water.

Our goal was to develop an IR spectroscopy method that could overcome the limitations of existing Raman or IR spectroscopy implementations and improve the sensitivity and accuracy achieved in determining solute concentrations in aqueous solution. We hypothesized that we could improve the sensitivity of optoacoustic spectroscopy by minimizing the contributions of water using temperature modulation of the sample being examined. This hypothesis is based on a long-known property of the thermal expansion coefficient of water, which becomes zero at 4 °C (29). The dependence of optoacoustic signal on temperature has been experimentally demonstrated in the NIR spectral region (700 to 900 nm) (22, 30–32).

To investigate the validity of our hypothesis we developed a cooled IR optoacoustic spectroscopy (CIROAS) arrangement and applied it to record optoacoustic spectra of lipids, bovine serum albumin (BSA), and glucose in aqueous solution at different temperatures. We muted water contributions in the NIR-II region (900 to 1,900 nm), where sugars, lipids, and proteins emit strong optoacoustic signals, generally much stronger than in the NIR. Therefore, we aimed to remove the strong contributions from water on the signal collected in the NIR-II and detect these moieties with higher sensitivity. Measurements were performed over many wavelengths in the NIR-II region and compared the CIROAS detection sensitivity to conventional optoacoustic NIR-II spectroscopy at room temperature. To elucidate the CIROAS principle of operation, we studied how solute concentration influences 1) the muting point of an aqueous solution (temperature at which water signal is muted) and 2) the rate of change of optoacoustic signal with temperature. We further showcase that the rate of change of the OA signal as a function of temperature can be employed to quantitatively determine the solute concentration. We discuss how CIROAS may substantially extend the ability of optoacoustics to sense biological molecules in cells and tissues.

Methods

Theory. Generation of optoacoustic signal requires stress and thermal confinement criteria to be satisfied (22, 33, 34). Thermal and stress confinement conditions can be satisfied by having the pulse width of light excitation be shorter than thermal and stress relaxation times, respectively (33). Once these criteria are satisfied, the fractional volume expansion (dV/V) generated by the pulsed laser is written as (33)

$$\frac{dV}{V} = -\kappa \Delta p + \beta \Delta T, \quad [1]$$

where κ is the isothermal compressibility, β is the thermal expansion coefficient, and Δp and ΔT represent the changes in measured pressure and temperature, respectively.

When the pulse width is on the order of nanoseconds the heating is rapid, and the accompanying fractional volume expansion is negligible (i.e., $dV/V = 0$); therefore, the local pressure rise after the laser excitation pulse will be (33)

$$\Delta p = \frac{\beta \Delta T}{\kappa} = \frac{\beta}{\kappa \rho C_v} H = \Gamma H, \quad [2]$$

where ρ is the mass density, C_v represents the specific heat capacity at constant volume, and H is the absorbed optical energy density. Furthermore, the dimensionless Grueneisen parameter (Γ) can be defined as (33)

$$\Gamma = \frac{\beta}{\kappa \rho C_v} = \frac{\beta v^2}{C_p} = g(T), \quad [3]$$

where v is the speed of sound, C_p indicates the specific heat capacity at constant pressure, and T represents temperature of the medium being probed. Therefore,

$$\Delta p = g(T) H. \quad [4]$$

The pressure rise (optoacoustic signal) is a function of temperature of the object under investigation (as seen in Eq. **4**). Thus, prior works have used the generated optoacoustic signal during laser excitation for monitoring the temperature of the medium (35). Given that the instantaneous temperature increase in the medium due to the laser pulse heating is of the order of millikelvins (33), the laser pulse heating will not affect the Grueneisen parameter value. Notably, the thermal expansion coefficient β is related to the temperature through the following relation (30):

$$\beta = \beta_1 + \beta_2 T, \quad [5]$$

where β_1 and β_2 are the first two coefficients in a power (Taylor) series expansion of β. Eqs. **3–5** are combined to yield

$$\Delta p = \frac{(\beta_1 + \beta_2 T) v_s^2}{C_p} H. \quad [6]$$

Interestingly, $\beta_{water} = 0$ for water at 4 °C (29, 36), resulting in zero optoacoustic signal (i.e., water is optoacoustically mute). When the temperature is reduced further, β_{water} becomes negative, leading to a reversed optoacoustic signal, with the physical meaning that the optoacoustic point source first contracts and then expands upon excitation. In contrast, at temperatures above 4 °C, β_{water} is monotonic and positive, leading to generation of an optoacoustic signal with the expected bipolar signal (i.e., positive peak followed by negative peak).

The underlying CIROAS premise is that the presence of target solutes in water (such as lipids, proteins, or sugars) would alter the temperature dependence of the optoacoustic signal generated by the solute compared to water, by changing the thermal expansion coefficient of the aqueous solution. The thermal expansion coefficient of the aqueous solution can be written as

$$\beta_{aqueous} = \beta_{water} + \Delta\beta. \quad [7]$$

The generated optoacoustic signal can then be written as

$$\Delta p = \beta_{aqueous} \frac{v_s^2}{C_p} H = (\beta_{water} + \Delta\beta) \frac{v_s^2}{C_p} H. \quad [8]$$

Assuming the coefficients of the Taylor series are similar in water and aqueous solution, our aim is to demonstrate that the variations in the muting point could be potentially used to measure the concentration of the sample being investigated. Notably, the shift in the muting temperature of a solute vs. the muting temperature of water (i.e., 4 °C) as a function of solute concentration is given by the Despretz law (i.e., $\Delta T = Kc$), where K is the Despretz constant and c is the solute concentration (32, 37). Here, ΔT represents a small change in the temperature from 4 °C to the actual muting point in the presence of solutes. In the context of optoacoustics, we can rewrite the thermal expansion coefficient of the aqueous solution at muting temperature of solute $(T_{mute} + \Delta T)$ as

$$\beta_{aqueous} = \beta_1 + \beta_2 T = \beta_1 + \beta_2 (T_{mute} + \Delta T) = \beta_{water} + \beta_2 (\Delta T), \quad [9]$$

where T_{mute} indicates the muting point of water. Therefore at 4 °C, the optoacoustic signal from an aqueous solution is

$$\Delta p = \beta_{aqueous} \frac{v_s^2}{C_p} H = \beta_2 \Delta T \frac{v_s^2}{C_p} H. \quad [10]$$

We can rewrite Eq. **10** using the Despretz law at 4 °C as

$$\Delta p = \beta_2 K c \frac{v_s^2}{C_p} H. \quad [11]$$

Eq. **11** indicates that the optoacoustic pressure detected at water muting temperature is proportional to the solute concentration and can be therefore used for quantitative spectroscopy purposes. We were particularly interested herein identifying the use of Eq. **11** in the SWIR spectral region. Quantifying the changes in the optoacoustic signal intensity at SWIR excitation wavelengths at which the solute target strongly absorbs, under water muting conditions, could allow an accurate determination of target concentration with higher sensitivity than in the NIR.

Experimental Setup. The CIROAS system (Fig. 1) employed the illumination of a tuneable nanosecond SpitLight Single OPO laser (Innolas). The output power was set to 0.5 mJ across the whole NIR-II spectral range of 900 to 1,900 nm. The wavelength scanning step was set to 10 nm. A cylindrically focused ultrasonic transducer (UST) with a 7.5-MHz central frequency (V319;

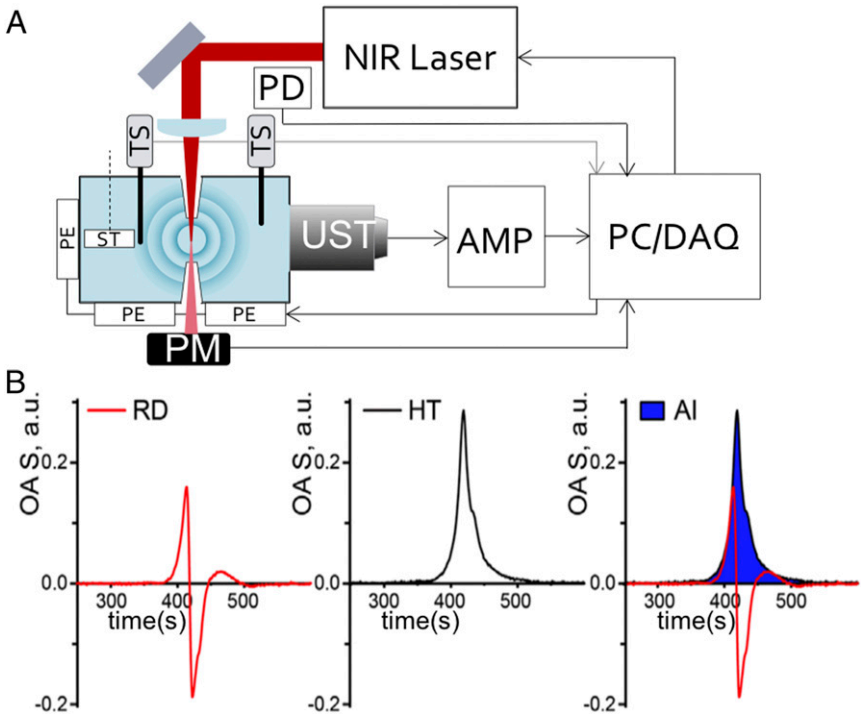

Fig. 1. (*A*) Schematic representation of the experimental setup for optoacoustic spectroscopy. UST, ultrasound transducer; PD, photodiode; AMP, amplifier; TS, temperature sensor; PM, power meter; ST, stirrer; PE, Peltier element; PC/DAQ, personal computer with data acquisition card. (*B*) Data processing and analysis steps. OAS raw data (RD, *Left*) was transformed by Hilbert transformation (HT, *Middle*), and the area of interest (AI, *Right* in blue) under curves was taken as the intensity of the OAS signal (I_{OA}).

Olympus Panametrics-NDT) was used for detecting the generated optoacoustic signal. The UST was adjusted to accommodate the beam in its focus. Acquired signals first were amplified with a low noise amplifier (AU-1291; Miteq Inc.) then digitized using a fast data acquisition card (DAQ) operating at 100 MS/s (EON-121-G20, Gage Applied Technologies). Simultaneously, the intensity of light passed through the medium was registered by a power meter and the values were used to calculate the optical absorption. A trigger signal from the photodiode was used to synchronize the detection in DAQ. To measure OA spectra at different temperatures a measurement chamber was built, where temperature was controlled using Peltier elements (Fig. 1). Six thermocouple-based temperature sensors were placed inside the chamber to provide accurate reading of the temperature. The average value of measured temperature was used in closed-loop configuration to control the Peltier elements, maintaining the desired temperature. During all measurements, a mechanical stirrer was constantly mixing the solution to ensure homogeneous temperature throughout the measurement chamber.

Data collection and processing. Data acquisition and processing were performed in MATLAB (MathWorks). Obtained raw signal intensities were normalized per laser energy as registered by the power meter. The strength of the optoacoustic signal (I_{OA}) was estimated by computing the Hilbert transform of the recorded acoustic signal of each measurement and integrating the area under the curve (Fig. 1*B*) as previously suggested (27). For each wavelength, 40 optoacoustic measurements were recorded and averaged to increase SNR.

Experimental Measurements. To examine the merits of CIROAS we performed measurements of an aqueous solution at different temperatures ranging from 1.4 to 25.8 °C, using 1,440-nm illumination. The raw optoacoustic signals and the muting temperature were recorded in these experiments. Then, we examined the CIROAS's ability to measure glucose in the NIR-II region, as an application example. We investigated if glucose detection could be improved over conventional SWIR spectroscopy, by reducing the temperature of the medium being investigated. For this reason we prepared a stock solution of D(+)glucose ($C_6H_{12}O_6$; Merck) in distilled H_2O and added it to the test chamber in five titrations, covering a concentration range of 0 to 452 mg/dL. The test chamber contained 14 mL distilled H_2O. With each step of titration, aliquots of 1 mL of solution were first dispensed into the test reservoir, followed by addition of 1 mL of concentrated glucose stock solution. We also performed CIROAS measurements of a glucose in serum solution at 160, 120, 80, 45, and 30 mg/dL glucose concentrations. Serum was provided by filtering BSA with a 0.4-μm filter. CIROAS glucose measurements were compared to measurements of the same solution by a glucometer (Contour Next One). As a second application example, we performed CIROAS measurements from a lipid solution, prepared by mixing Intralipid (20% emulsion, I141-100ML; Sigma) and water (14). Finally, a third example demonstration was investigated by using 50 g/L BSA solution, which represents a physiologically relevant protein concentration.

Results

We investigated the optoacoustic signal detected from water as a function of temperature. We were particularly interested to study the muting property in water measured at the SWIR spectral window and to confirm our hypothesis that CIROAS of biomolecules in this wavelength range can offer accurate detection with increased sensitivity over regular spectroscopy. Fig. 2*A* shows the dependence of the optoacoustic signal on temperature, using illumination at 1,440 nm, and depicts a decline of intensity with reducing temperature until the signal becomes undetectable (mute) at 4 °C. Further reduction in temperature leads to the appearance of optoacoustic response, but with an inverted profile (Fig. 2*B*, signal at 1.8 °C), that is, the negative peak precedes the positive one for signals recorded at temperatures below 4 °C, in contrast to signals collected above 4 °C (Fig. 2*C*, signal at 21 °C). Fig. 2*D* presents the optoacoustic spectrum recorded at different temperatures from water at illumination wavelengths in the range of 900 to 1,840 nm. At 4 °C, the entire spectrum is near baseline, as expected, indicating that water becomes optoacoustically mute in the SWIR region despite its strong absorption in this wavelength range. These measurements therefore report on the change of polarity of the optoacoustic signal for temperatures below 4 °C and the muting of the optoacoustic response in the SWIR.

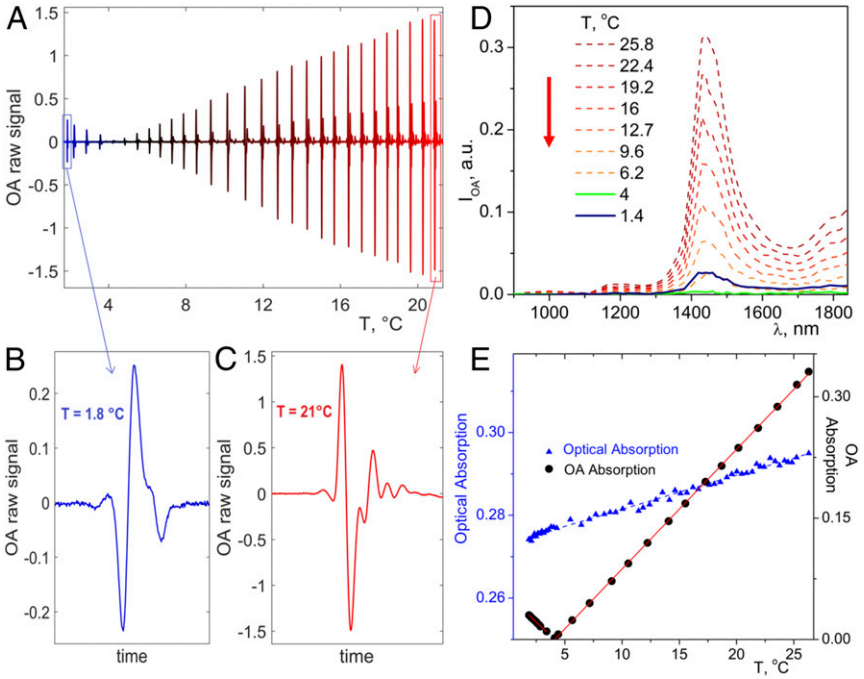

Fig. 2. Optoacoustic signal of pure water at different temperatures after illumination in the SWIR range. (*A*) Raw optoacoustic signal of water at different temperatures after illumination at 1,440 nm. (*B*) Temporal raw optoacoustic signal at 1.8 °C. (*C*) Temporal raw optoacoustic signal at 21 °C. (*D*) Optoacoustic spectra of water at different temperatures after illumination in the SWIR range. (*E*) Comparison of the signal obtained from pure water at different temperatures after illumination at 1,440 nm using optical and optoacoustic measurements.

Fig. 2*E* depicts optical and optoacoustic signals recorded from pure water at the temperature range of 1.4 to 25.8 °C, using 1,440-nm illumination. The optical signal was recorded as an attenuation signal in transmission mode and is plotted as an absorption curve using the Beer–Lambert law. The change of water absorption recorded with the optical measurement exhibits a minor slope of 0.001/°C with temperature. In contrast, the optoacoustic signal changes significantly (slope = 0.02/°C). This graph confirms the potential advantage of using optoacoustic spectroscopy over OS at reduced temperature. In particular, strong water absorption in the SWIR can overshadow the contributions from the absorption of other molecules in a solution. However, using the water-muting property in the SWIR, it is possible to significantly reduce the contributions of water on the optoacoustic signal. Consequently, we then investigated whether the detection sensitivity of cooled optoacoustic spectroscopy could be increased for sensing optically absorbing molecules in aqueous solution at 4 °C, over conventional OS.

Following the comparison between optical and optoacoustic measurements, we examined the CIROAS application to measuring solutes (Fig. 3). Fig. 3*A* shows the raw optoacoustic signal recorded from an aqueous solution of glucose (452.2 mg/dL) after illumination at 1,580 nm as a function of temperature ranging from 0.6 to 18.5 °C. Fig. 3*A*, *Inset* zooms in the signal at 4 °C and allows a first insight that the muting point of the glucose solution is shifted at lower temperatures than 4 °C, that is, lower than the muting point for pure water. This observation is better shown in Fig. 3*B*, which plots the raw optoacoustic signals measured at 1,580 nm from pure water and aqueous solution of glucose at ∼4 °C. We observe that, in contrast to pure water, the glucose solution shows detectable optoacoustic signal at 4 °C with normal polarity, due to the change in thermal expansion coefficient of the water in the presence of solutes such as glucose, lipid, or proteins.

We then examined the relative spectra measured at 4 °C from pure water and from the glucose aqueous solution at 452.2 mg/dL glucose concentration. Fig. 3*C* shows the optoacoustic SWIR spectra measured and demonstrates that while the pure water spectrum is close to baseline (as also shown in Fig. 2) the spectrum from the glucose aqueous solution yields a stronger signal as seen in the graph. Further, to examine whether cooling improves the detection characteristics of glucose over room temperature we plotted normalized OA spectra of water at 18 °C and of aqueous solution of glucose at 18 °C (Fig. 3*D*). The comparison reveals that there are differences between the pure water and glucose solution spectra especially at a 1,550- to 1,700-nm spectral window. Fig. 3*D* indicates that the spectra of water and glucose at 18 °C are very similar, due to the strong contribution of the water absorption. However, when we compare the spectrum of water and aqueous solution of glucose at 4 °C, we observe the characteristic difference at the 1,550- to 1,700-nm spectral window also seen in Fig. 3*C*. Fig. 3*E* shows the optoacoustic spectra of aqueous solutions of glucose recorded at different temperatures. Consistent with the preliminary observation in Fig. 3*A*, we see that the aqueous solution of glucose gives appreciable signal at 4 °C with a maximum at ∼1,440 nm, whereas pure water gives negligible signal (Fig. 2*D*). Further, we can observe in Fig. 3*E* that the acquired OA spectrum goes to the baseline (close to 0, indicated in green) at 3.1 °C, which means the muting point has shifted to a lower temperature than 4 °C. Fig. 3*E* also indicates that substantial OA signal was detected when temperature was further reduced to 1.5 °C, which is indicated in blue. Finally, Fig. 3*F* shows spectra corresponding to glucose measurements at different temperatures. All spectra shown have been processed by subtracting the water contribution. However, since the water spectrum gives minimum optoacoustic contribution at the muting point (4 °C), the subtraction of all water–glucose spectra obtained at different temperatures was performed using the normalized OA water spectrum at 18 °C. Fig. 3*F* demonstrates that CIROAS yields more sensitive measurements of glucose as the temperature reduces to 4 °C, specifically at 1,550 to 1,700 nm.

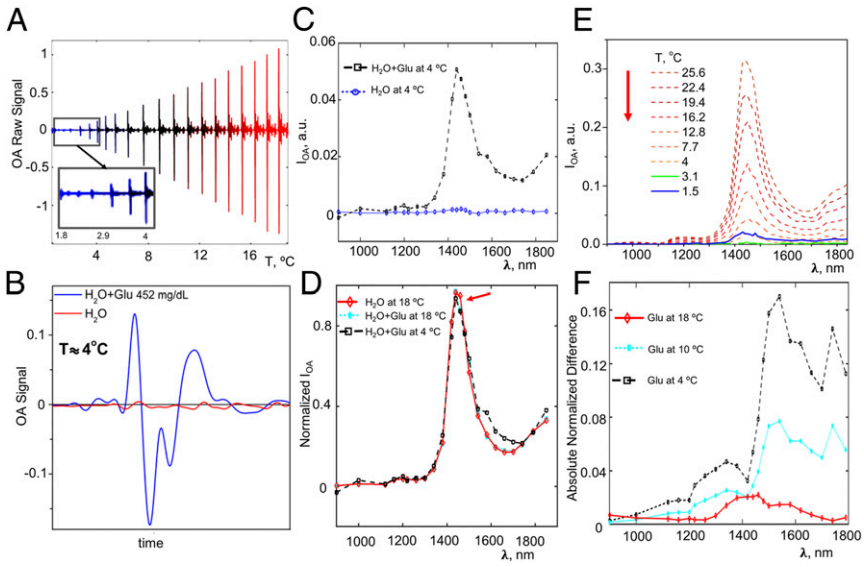

Fig. 3. Optoacoustic signal of an aqueous solution of glucose (452.2 mg/dL) at different temperatures after illumination in the SWIR range. (*A*) Raw optoacoustic signal at temperatures between 0.6 and 18.5 °C after illumination at 1,580 nm. (*B*) Superposition of the optoacoustic signals of pure water (red line) and the aqueous solution of glucose (blue line) at 4 °C. (*C*) Optoacoustic spectra of pure water at 4 °C (dotted blue line) and the aqueous solution of glucose (dashed black line) at 4 °C. (*D*) Normalized optoacoustic spectra of pure water (solid red), aqueous solution of glucose at 18 °C (dotted cyan), and aqueous solution of glucose at 4 °C (dash black). (*E*) Optoacoustic spectra of the aqueous solution of glucose at different temperatures after illumination in the SWIR range. (*F*) OA signal from glucose, calculated as the normalized difference between the OA measurements at 4 °C, 10 °C, and 18 °C and the water spectrum at room temperature.

Repeated measurements of OA spectra from aqueous solution of glucose were performed to examine the CIROAS reproducibility (*SI Appendix*, Fig. S1). We observed normalized OA spectra corresponding to pure water at 25 °C, glucose solution (400 mg/dL) at 4 °C, and saturated glucose solution, the latter prepared by continuously adding glucose in heated water until glucose could not be further dissolved. A clear difference between pure water spectrum and glucose solution spectrum at the 1,550- to 1,700-nm spectral window can be seen in *SI Appendix*, Fig. S1, a result similar to the observation in Fig. 3 *C* and *D*. There are some small differences observed in the shape between the OA spectra from aqueous solution of glucose in Fig. 3*D* and *SI Appendix*, Fig. S1, possibly due to differences in the water spectrum between 18 °C and 25 °C and measurement error. Interestingly, the OA spectral measurements at the 1,550- to 1,700-nm spectral window in *SI Appendix*, Fig. S1 reveal that at higher concentration (i.e., saturated glucose) the deviation in normalized OA signal is higher compared to measurements of glucose solution at physiological concentration (i.e., 400 mg/dL and 4 °C). To investigate the possible presence of nonlinearity in the measurement, we measured the OA signal as a function of glucose concentration. Measurements at different wavelengths (*SI Appendix*, Fig. S1) indeed showed a nonlinear behavior, with recorded signals nonlinearly increasing at higher concentration. This behavior was further found to be wavelength-dependent. This nonlinear variation may further explain the deviation in OA spectra of saturated glucose compared to OA glucose spectra at physiological concentration. Such nonlinear behavior has been previously noted (38) and was attributed to optical absorption saturation effects.

As a next step, we examined how changing the glucose concentration alters the muting point and the OA signal dependence on temperature. Such dependence would be in analogy to how solute concentration changes the boiling or the freezing temperature point relative to the value for pure solvent. We performed measurements with glucose solutions in water ranging in concentration from 50 to 600 mg/dL. Representative data at 149.6 and 452.2 mg/dL are shown in Fig. 4 and illustrate a temperature dependence of the OA signal intensity at 1,580 nm for pure water and for aqueous solutions of glucose. Overall, the range examined covers normal and hyperglycemic levels reported in brain and blood (3, 39, 40). Linear fits to data show monotonic increases with temperature. The fitted lines intersect with the temperature axis at 4 °C for pure water, 3.7 °C for water containing glucose at 149.6 mg/dL, and 3.1 °C for water containing glucose at 452.2 mg/dL. The corresponding slopes of fitted lines were 0.0582, 0.0538, and 0.0527 (change in OA signal per °C). These results indicate that both the temperature intercept and OA signal–temperature slope varied proportionally with glucose concentration. This dependence can be therefore employed for quantifying the concentration of biomolecules in solutions.

We further observed the limit of detection (LoD) for glucose in water, by investigating the minimum amount of glucose that imparted a measurable change in the muting point. We found that 50 mg/dL (Fig. 4*B*) was a reliably observed minimum change. Smaller changes in concentration amounts resulted in muting point variations of ∼0.06 °C, which could not be accurately controlled by the current implementation of the CIROAS setup. Correspondingly, the LoD measurements for glucose in serum was found to be 45 mg/dL (Fig. 4*C*). However, the sensitivity of the system when adding a small amount of glucose in an existing glucose –water solution was found to be better than LoD, at 8 mg/dL. In other words, while the minimum detection point when adding glucose to pure water was 50 mg/dL for water solution (45 mg/dL for serum), the minimum change detected when adding glucose to a water–glucose solution at 136 mg/dL glucose concentration was only 8 mg/dL (*SI Appendix*, Fig. S3) and defines the sensitivity of the current CIROAS setup to glucose changes. Comparison of the CIROAS glucose concentration measurements to glucometer measurements are summarized in *SI Appendix*, Table S1. The comparison reveals that CIROAS outperformed the commercial glucometer device, since it better predicted the known glucose concentration in the solution measured.

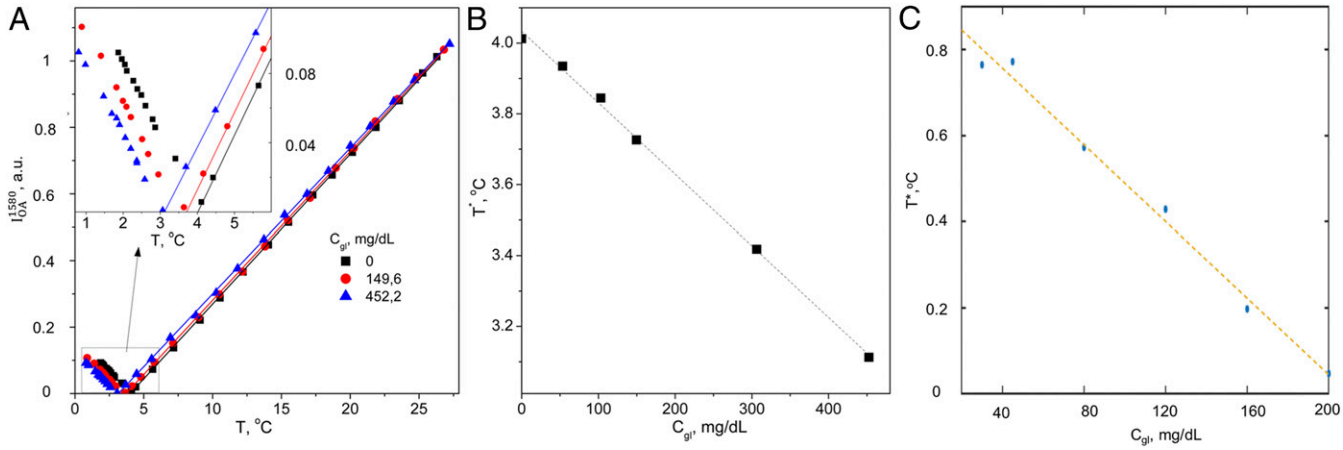

Fig. 4. Temperature dependence of optoacoustic signal measured from water as a function of solute concentration. (*A*) Temperature dependence of optoacoustic signal intensity of pure water (black squares) and aqueous solutions of glucose at 149.6 mg/dL (red circles) or 452.2 mg/dL (blue triangles). Linear fitting of monotonically increasing signals is shown. (*Inset*) The muting point of each solution, defined as the intersection with the temperature axis. (*B*) Variation in muting point (T*) with glucose concentration (Cgl). (*C*) Variation in muting point (T*) with glucose concentration (Cgl) in serum solution.

We further examined CIROAS of lipid and protein detection compared to measurements at room temperature. Fig. 5*A* shows measured OA spectra from 890 nm to 1,000 nm for aqueous solution of lipids at different temperatures. This wavelength range was chosen because lipid shows a distinct peak at 930 nm, while water shows a peak at 970 nm. We observe that the 930-nm peak becomes visible at lower temperatures, but it is not prominent as we increase the temperature. We also observed that the OA signal continues to decrease as the temperature reduces below 4 °C. This signal decrease might be due to interference and OA signal cancellation between lipid (positive peak preceding negative peak below 4 °C) and water (negative peak preceding positive peak below 4 °C). Note that similar behavior was not observed while probing glucose solution; this may be because glucose is readily soluble in water compared to lipid molecules causing interference of the OA signals from lipid and water. Fig. 5*B* indicates the normalized OA measurements [i.e., $x/\max(x)$, where x is the acquired OA spectrum] from lipid solution at 19 °C and 4 °C, showing the spectral difference of the lipid solution at the two temperatures. Fig. 5*C* depicts the ratio

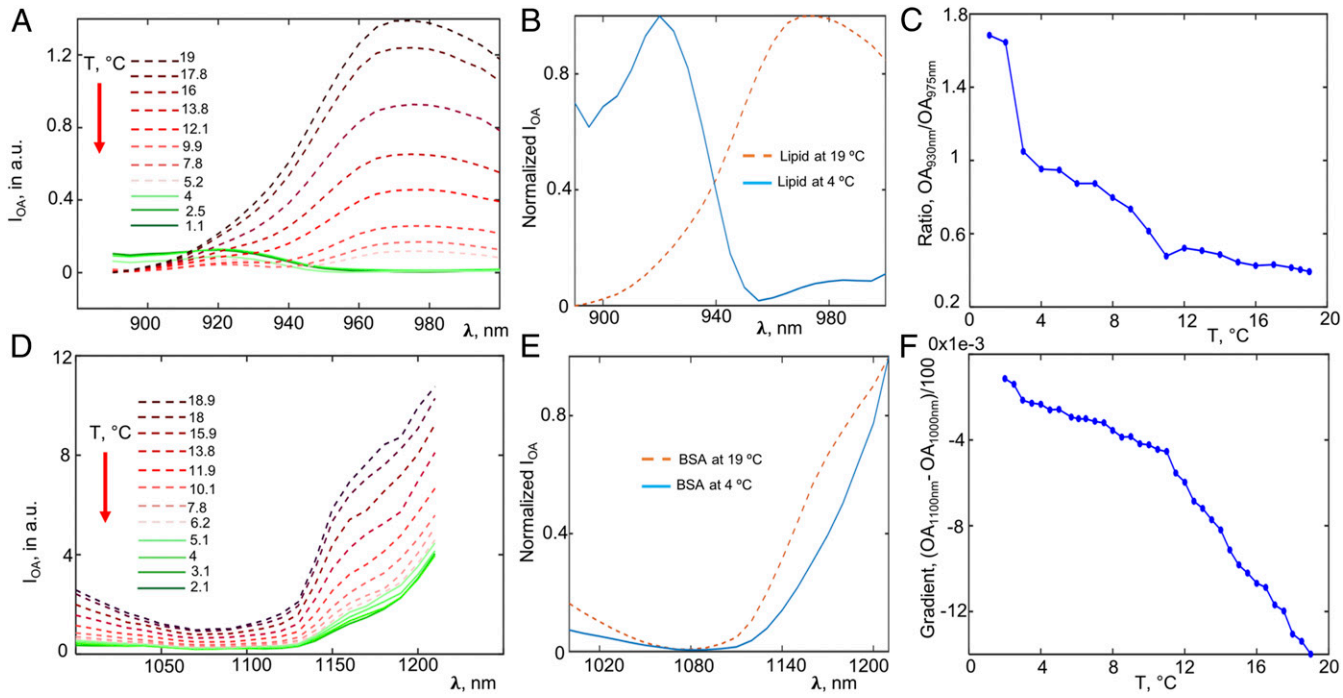

Fig. 5. Optoacoustic signal of an aqueous solution of lipid (10%) and BSA (50 g/L) at different temperatures after illumination in the SWIR range. (*A*) Optoacoustic spectra of lipids in aqueous solution at different temperatures after illumination in the wavelength range of 890 to 1,000 nm. (*B*) Comparison of normalized OA spectra of lipid solution at 19 °C (dotted orange line) and at 4 °C (solid blue line). (*C*) Ratio of optoacoustic signal from the lipid solution at 930 nm (lipid peak) to signal at 970 nm (water peak) at different temperatures. (*D*) Optoacoustic spectra of BSA in aqueous solution at different temperatures after illumination in the wavelength range of 1,000 to 1,210 nm. (*E*) Comparison of normalized OA spectra of BSA solution at 19 °C (dotted orange line) and at 4 °C (solid blue line). (*F*) Gradient in the measured optoacoustic signal from BSA solution between 1,000 and 1,100 nm at different temperatures.

of the measured OA signal at 930 nm to that of 970 nm as a function of temperature for the measurements shown in Fig. 5*A*. The curve shows that the relative signal obtained primarily due to lipid contributions at 930 nm becomes four times stronger at lower temperatures compared to the signal obtained at 970 nm, which is primarily attributed to water absorption. This observation suggests a four times lipid detection sensitivity improvement at lower temperatures.

Fig. 5*D* indicates the measured OA spectra from 1,000 to 1,210 nm for an aqueous solution of BSA at different temperatures. BSA does not exhibit characteristic peaks in the measured wavelength range, but between 1,000 and 1,100 nm BSA shows a roughly constant absorption, whereas water decreases in absorption with increasing wavelength. Therefore, at lower temperatures, we clearly see a decrease in OA signal intensity and a flattening of the spectrum in the 1,000- to 1,100-nm range, reflecting the water muting effects. Fig. 5*E* plots the normalized measurements from BSA solution at 19 °C and 4 °C, showcasing the spectral differences at the two temperatures. At 4°, the BSA solution shows a reduced signal compared to 18°, due to the reduction of water absorption contribution to the OA signal.

An analysis similar to the one performed in Fig. 5*C* shows that the gradient of the optoacoustic signals obtained between 1,000 nm and 1,100 nm from the BSA solution decreases with reducing temperature. The gradient used in Fig. 5*F* is calculated using $(y_{1,100} - y_{1,000})/100$, where $y_{1,100}$ is the OA signal from BSA solution at 1,100 nm and $y_{1,000}$ is the OA signal from BSA solution at 1,000 nm. Note that we used a ratio of spectral peaks for the lipid measurement (Fig. 5*C*) since the lipids have a distinct peak at 930 nm, whereas water has a peak at 970 nm. However, we used the gradient calculation in Fig. 5*F*, since the BSA spectrum does not have such distinct peaks in its spectrum. The gradient measure tends to be closer to 0 at lower temperatures, indicating that the BSA spectral signature dominates at lower temperatures, but water contributions begin to appear with increasing temperature. The BSA detection sensitivity is five times greater at lower temperatures compared to higher temperatures.

We also examined the muting points for lipid and protein. In contrast to the glucose measurements, whereby the muting point was same at all wavelengths, *SI Appendix*, Fig. S2 *A* and *B* show that the muting point of lipid solution was higher at 930 nm (i.e., about 8 °C) compared to 970 nm (where the muting point was at 2.5 °C). Moreover, *SI Appendix*, Fig. S2*C* shows the muting point of BSA solution at 1,070 nm, found to be at 1.8 °C; however, the OA signal at higher wavelengths did not mute at all, as can be seen from Fig. 5*D*. Currently we investigate the variation of thermal expansion coefficient as a function of temperature for biomolecules such as glucose, lipids, and proteins in order to gain better insights into these muting point variations, along the lines of Eqs. **9**–**11**. Finally, LoD and sensitivity measurements were also performed for the lipid solution. We found the LoD for lipid to be 2% of Intralipid solution, using the current CIROAS setup, while the sensitivity of lipid detection, that is, the minimum change that could be observed in our setup, was 1% of Intralipid solution. Lipid LoD and sensitivity was determined as the minimum change of the ratio of the OA signal at 930 nm to the OA signal at 975 nm that could be reliably obtained using the CIROAS setup (*SI Appendix*, Fig. S4).

Discussion

We exploited the dependence of optoacoustic signals on temperature for improving the sensitivity of IR spectroscopy. Compared to measurements at room temperature, CIROAS at 4 °C yielded on average a fivefold sensitivity improvement in the SWIR over measurements at room temperature. These improvements can be observed as more pronounced spectral differences in the glucose spectrum (e.g., Fig. 3*F*) or as relative changes for lipids and BSA, that is, with respect to the ratio OA_{930}/OA_{975} in the case of lipid and the per-wavelength normalized difference $(OA_{1,100} - OA_{1,000})/100$ in the case of BSA. We explored the modifications of the muting point as a function of solute concentration and measured OA signal as a function of temperature for a carbohydrate, a protein, and a lipid solution. Previously, temperature dependence of the optoacoustic signal has been utilized for determining the temperature of a sample, for example during thermal therapy using focused ultrasound (41, 42) or while ablating tissue with a laser fiber (35, 43). This dependency has also been used to discriminate nonlinear optoacoustic emission of gold nanospheres dissolved in water from the linear optical absorption of the water solvent in the NIR-I region (44). However, the effects of muting water responses at about the 4 °C temperature has not been previously explored. By exploiting this muting property, we show therefore a spectroscopic approach and demonstrate benefits in utilizing optoacoustic readings over conventional optical readings, common in IR spectroscopy.

Our demonstration and analysis focus on the IR wavelengths, and in particular in the SWIR range, and address the long-standing problem of strong light absorption by water in this spectral region that challenges the detection sensitivity. Moreover, it has been particularly difficult to detect metabolites such as glucose, since both water and glucose molecules have an O–H group, giving rise to a similar spectrum with a strong absorption peak at 1,440 nm. As per Fig. 2, we can conclude that the generated OA signal from water below 4 °C changes its polarity, that is, the negative peak will be followed by the positive peak (because the thermal expansion coefficient becomes negative). Conversely, the OA signal generated from glucose retains the sequence of a positive peak followed by negative peak at temperatures below 4 °C. As a result, there would be interaction of these two OA signals, generated due to water and glucose molecules, resulting in shifting of the muting point to 3 °C (below 4 °C). By lowering the temperature and muting the contributions of water, we enable more sensitive spectroscopic detection of glucose and possibly other biomolecules, as elaborated in Figs. 3–5.

We provide evidence that the "muting point" can be observed at all SWIR wavelengths and represents an essential CIROAS feature that allows up to fivefold improved sensitivity in biomolecule detection compared to room-temperature spectroscopy. For the glucose solution, the exact muting point and the slope of thermal dependence of optoacoustic signal were shown to depend on glucose concentration. This trend could be modeled by assuming a thermal expansion coefficient β that depends on solute concentration (Eqs. **10** and **11**) analogously to other colligative properties of water, such as boiling point, freezing point, and vapor pressure (45, 46). We show that the dependence of muting point on the solute concentration can be employed to quantify the concentration of biologically relevant solutes, that is, CIROAS measurements at different temperatures can be employed for quantifying the concentration of solutes in aqueous solutions. The results further show that besides glucose CIROAS improves the sensitivity of detection of protein and lipid, which opens up the possibility of improving detection of many other biomolecules, such as lactose, sucrose, galactose, cathepsin, integrin, and myosin. Optoacoustic measurements in the SWIR spectral range are unaffected by other abundant but weakly absorbing chromophores such as hemoglobin and melanin, making CIROAS an attractive method for measurements of metabolites in solution.

CIROAS involves changing the temperature, which alters the speed of sound (47, 48), thereby changing the calculated position of the optoacoustic source. However, the change in position should not pose a problem for quantitation of solutes in homogeneous solution. Nevertheless, accurate determination of the speed of sound may be useful, especially since it can allow an

estimation of sample temperature (49) during solute quantification or spectral analysis or in imaging applications (50). CIROAS appears to be superior to alternative optical spectroscopic methods that use heavy water as the means to overcome the effects of strong water absorption (8). Besides being impractical and cost-ineffective, the use of heavy water is not compatible with measuring biological samples that consist of >80% of water.

Broad implementation of CIROAS will require hardware that allows varying the temperature of the sample, using a Peltier element or other means. Such implementations are widely available, and they do not represent a technological barrier. Therefore, CIROAS can enable a spectroscopic approach with high dissemination potential, offering a straightforward way to improve the sensitivity of detection of various molecules in biological samples. The method can be employed for conventional laboratory measurements or for analyzing biological fluids, such as blood measurements. Miniaturization of components is also technically straightforward, which implies applications in conventional spectroscopy or as part of microfluidic and laboratory-on-a-chip measurement setup. In the future, imaging implementations using two- or three-dimensional optoacoustic scans can be also contemplated.

Data Availability. The data used in this paper are deposited in ref. 51, and the corresponding codes to analyze the data can be found in ref. 52.

ACKNOWLEDGMENTS. J.P. acknowledges support from Alexander von Humboldt postdoctoral fellowship program. V.N. acknowledges the SENSE4-LIFE project funded by the Federal Ministry of Education and Research, and the Horizon 2020 Innovative Dermatology Healthcare (INNODERM) funding program. We thank Dr. Chapin Rodriguez for insightful comments.

1. P. Libby, P. M. Ridker, A. Maseri, Inflammation and atherosclerosis. *Circulation* **105**, 1135–1143 (2002).
2. L. S. Eberlin *et al*., Classifying human brain tumors by lipid imaging with mass spectrometry. *Cancer Res.* **72**, 645–654 (2012).
3. N. Marty, M. Dallaporta, B. Thorens, B. Thorens, Brain glucose sensing, counter-regulation, and energy homeostasis. *Physiology (Bethesda)* **22**, 241–251 (2007).
4. American Diabetes Association, Diagnosis and classification of diabetes mellitus. *Diabetes Care* **34** (suppl. 1), S62–S69 (2011).
5. E. B. Hanlon *et al*., Prospects for in vivo Raman spectroscopy. *Phys. Med. Biol.* **45**, R1–R59 (2000).
6. A. Glinzer *et al*., Targeting elastase for molecular imaging of early atherosclerotic lesions. *Arterioscler. Thromb. Vasc. Biol.* **37**, 525–533 (2017).
7. X. Ma *et al*., Integrin-targeted hybrid fluorescence molecular tomography/X-ray computed tomography for imaging tumor progression and early response in non-small cell lung cancer. *Neoplasia* **19**, 8–16 (2017).
8. Q. Cao, N. G. Zhegalova, S. T. Wang, W. J. Akers, M. Y. Berezin, Multispectral imaging in the extended near-infrared window based on endogenous chromophores. *J. Biomed. Opt.* **18**, 101318 (2013).
9. G. Hong *et al*., Through-skull fluorescence imaging of the brain in a new near-infrared window. *Nat. Photonics* **8**, 723–730 (2014).
10. R. Pandey *et al*., Noninvasive monitoring of blood glucose with raman spectroscopy. *Acc. Chem. Res.* **50**, 264–272 (2017).
11. K. Weinger, A. M. Jacobson, M. T. Draelos, D. M. Finkelstein, D. C. Simonson, Blood glucose estimation and symptoms during hyperglycemia and hypoglycemia in patients with insulin-dependent diabetes mellitus. *Am. J. Med.* **98**, 22–31 (1995).
12. H. W. Siesler, Y. Ozaki, S. Kawata, H. M. Heise, *Near-Infrared Spectroscopy: Principles, Instruments, Applications* (Wiley-VCH, Weinheim, 2002).
13. P. Larkin, *Infrared and Raman Spectroscopy: Principles and Spectral Interpretation* (Elsevier, ed. 2, 2017).
14. A. T. Buss, N. Fox, D. A. Boas, J. P. Spencer, Probing the early development of visual working memory capacity with functional near-infrared spectroscopy. *Neuroimage* **85**, 314–325 (2014).
15. S. L. Jacques, Optical properties of biological tissues: A review. *Phys. Med. Biol.* **58**, R37–R61 (2013).
16. G. A. Wagnières, W. M. Star, B. C. Wilson, In vivo fluorescence spectroscopy and imaging for oncological applications. *Photochem. Photobiol.* **68**, 603–632 (1998).
17. R. L. Mccerry, *Raman Spectroscopy in Chemical Bioanalysis* (John Wiley & Sons, 2005).
18. K. Kneipp, H. Kneipp, I. Itzkan, R. R. Dasari, M. S. Feld, Ultrasensitive chemical analysis by Raman spectroscopy. *Chem. Rev.* **99**, 2957–2976 (1999).
19. V. Gujrati, A. Mishra, V. Ntziachristos, Molecular imaging probes for multi-spectral optoacoustic tomography. *Chem. Commun. (Camb.)* **53**, 4653–4672 (2017).
20. J. Laufer, D. Delpy, C. Elwell, P. Beard, Quantitative spatially resolved measurement of tissue chromophore concentrations using photoacoustic spectroscopy: Application to the measurement of blood oxygenation and haemoglobin concentration. *Phys. Med. Biol.* **52**, 141–168 (2007).
21. A. C. Tam, Applications of photoacoustic sensing techniques. *Rev. Mod. Phys.* **58**, 381 (1986).
22. A. Rosencwaig, Photoacoustic spectroscopy of biological materials. *Science* **181**, 657–658 (1973).
23. G. P. Luke, S. Y. Nam, S. Y. Emelianov, Optical wavelength selection for improved spectroscopic photoacoustic imaging. *Photoacoustics* **1**, 36–42 (2013).
24. T. A. Filimonova, D. S. Volkov, M. A. Proskurnin, I. M. Pelivanov, Optoacoustic spectroscopy for real-time monitoring of strongly light-absorbing solutions in applications to analytical chemistry. *Photoacoustics* **1**, 54–61 (2013).
25. L. O. Usoltseva *et al*., Absorption spectra of nanodiamond aqueous dispersions by optical absorption and optoacoustic spectroscopies. *Photoacoustics* **12**, 55–66 (2018).
26. J. Kottmann, J. M. Rey, J. Luginbühl, E. Reichmann, M. W. Sigrist, Glucose sensing in human epidermis using mid-infrared photoacoustic detection. *Biomed. Opt. Express* **3**, 667–680 (2012).
27. A. Ghazaryan, M. Omar, G. J. Tserevelakis, V. Ntziachristos, Optoacoustic detection of tissue glycation. *Biomed. Opt. Express* **6**, 3149–3156 (2015).
28. A. Ghazaryan, S. V. Ovsepian, V. Ntziachristos, Extended near-infrared optoacoustic spectrometry for sensing physiological concentrations of glucose. *Front. Endocrinol. (Lausanne)* **9**, 112 (2018).
29. G. S. Kell, Precise representation of volume properties of water at one atmosphere. *J. Chem. Eng. Data* **12**, 66–69 (1967).
30. I. G. Calasso, W. Craig, G. J. Diebold, Photoacoustic point source. *Phys. Rev. Lett.* **86**, 3550–3553 (2001).
31. C. Li, L. V. Wang, Photoacoustic tomography and sensing in biomedicine. *Phys. Med. Biol.* **54**, R59–R97 (2009).
32. E. Petrova, A. Liopo, A. A. Oraevsky, S. A. Ermilov, Temperature-dependent optoacoustic response and transient through zero Grüneisen parameter in optically contrasted media. *Photoacoustics* **7**, 36–46 (2017).
33. L. V. Wang, H.-I. Wu, *Biomedical Optics: Principles and Imaging* (Wiley-Interscience, ed. 1, 2012).
34. P. Beard, Biomedical photoacoustic imaging. *Interface Focus* **1**, 602–631 (2011).
35. E. Bay, A. Douplik, D. Razansky, Optoacoustic monitoring of cutting efficiency and thermal damage during laser ablation. *Lasers Med. Sci.* **29**, 1029–1035 (2014).
36. M. F. Cawley, D. McGlynn, P. A. Mooney, Measurement of the temperature of density maximum of water solutions using a convective flow technique. *Int. J. Heat Mass Transfer* **49**, 1763–1772 (2006).
37. M. V. Kaulgud, W. K. Pokale, Measurement of the temperature of maximum density of aqueous solutions of some salts and acids. *J. Chem. Soc. Faraday Trans.* **91**, 999–1004 (1995).
38. A. Danielli, K. Maslov, C. P. Favazza, J. Xia, L. V. Wang, Nonlinear photoacoustic spectroscopy of hemoglobin. *Appl. Phys. Lett.* **106**, 203701 (2015).
39. G. Freckmann *et al*., Continuous glucose profiles in healthy subjects under everyday life conditions and after different meals. *J. Diabetes Sci. Technol.* **1**, 695–703 (2007).
40. A. J. Rose, E. A. Richter, Skeletal muscle glucose uptake during exercise: How is it regulated? *Physiology (Bethesda)* **20**, 260–270 (2005).
41. M. Kuniyil Ajith Singh, W. Steenbergen, Photoacoustic-guided focused ultrasound (PAFUSion) for identifying reflection artifacts in photoacoustic imaging. *Photoacoustics* **3**, 123–131 (2015).
42. Y. Sun, B. O'Neill, Imaging high-intensity focused ultrasound-induced tissue denaturation by multispectral photoacoustic method: An ex vivo study. *Appl. Opt.* **52**, 1764–1770 (2013).
43. G. A. Pang, E. Bay, X. L. Deán-Ben, D. Razansky, Three-dimensional optoacoustic monitoring of lesion formation in real time during radiofrequency catheter ablation. *J. Cardiovasc. Electrophysiol.* **26**, 339–345 (2015).
44. O. Simandoux, A. Prost, J. Gateau, E. Bossy, Influence of nanoscale temperature rises on photoacoustic generation: Discrimination between optical absorbers based on thermal nonlinearity at high frequency. *Photoacoustics* **3**, 20–25 (2014).
45. F. C. Andrews, Colligative properties of simple solutions. *Science* **194**, 567–571 (1976).
46. G. S. Manning, Limiting laws and counterion condensation in polyelectrolyte solutions. III. An analysis based on the Mayer ionic solution theory. *J. Chem. Phys.* **51**, 3249 (1969).
47. J. Jose *et al*., Speed-of-sound compensated photoacoustic tomography for accurate imaging. *Med. Phys.* **39**, 7262–7271 (2012).
48. S. Mandal, E. Nasonova, X. L. Deán-Ben, D. Razansky, Optimal self-calibration of tomographic reconstruction parameters in whole-body small animal optoacoustic imaging. *Photoacoustics* **2**, 128–136 (2014).
49. D. Van de Sompel, L. S. Sasportas, A. Dragulescu-Andrasi, S. Bohndiek, S. S. Gambhir, Improving image quality by accounting for changes in water temperature during a photoacoustic tomography scan. *PLoS One* **7**, e45337 (2012).
50. I. Steinberg *et al*., Photoacoustic clinical imaging. *Photoacoustics* **14**, 77–98 (2019).
51. J. Prakash, Short wavelength infrared optoacoustic spectroscopy based on water muting. Open Science Framework. https://osf.io/kt853/. Deposited 12 December 2019.
52. J. Prakash, Cooled IR optoacoustic spectroscopy based on water muting. GitHub. https://github.com/pnjayaprakash88/CIROAS_Spectroscopy.git. Deposited 13 December 2019.